Investigation of Nonlinear Optical Properties of Commercial Food Coloring Dye

Hasan Alfaraj

Department of Physics

University of Bahrain

Zallaq, Bahrain
hasan.a.alfaraj@gmail.com

Dr. Khalil Jasim
Department of Physics
University of Bahrain
Zallaq, Bahrain
kejasim@uob.edu.bh

Abstract—Natural organic dyes have been intensively investigated as nonlinear optical materials including saffron, curcumin, and hibiscus. However, the question of whether commercial food dyes exhibit nonlinear properties remains uncertain. In this study, we asked whether commercial food dyes exhibit nonlinear optical properties such as two-photon absorption, self-phase modulation, self-focusing, and self-defocusing effects. To answer this, the single beam Z-scan technique in two configurations known as closed and open aperture detectors were employed to measure the transmitted coherent beam in the direction of quantifying the third-order nonlinear susceptibility $\chi^{(3)}$. In both the open and closed aperture configurations, a thin sample of 1 mm thickness is translated through the optical axis of a continuous wave CW focused Gaussian laser beam emitted from an Arion laser system of wavelength 514 nm. Measurements were carried out on three levels of concentration and three different power levels. Two theoretical models are compared, the Gaussian decomposition model and the Thermal lens model. Dual beam spectrophotometer is used to measure linear optical absorption from which the linear absorption coefficient α was calculated. Fluorescence spectrum was recorded with computerized CDD spectrometer revealing peak intensity at emission wavelength of 630 nm. Normalized transmittance data was fitted using the Gaussian decomposition model to determine the phase distortion $\Delta\Phi_0$ and the on-axis nonlinear phase shift due to nonlinear absorption $\Delta\Psi_0$. Calculations of the nonlinear refractive index n_2 , nonlinear absorption coefficient β , and third-order nonlinear susceptibility $\chi^{(3)}$ for each concentration and power level are presented. Our results indicate that commercial yellow food dyes have a negative nonlinear refractive index n_2 attributed to selfdefocusing. Moreover, we report the observation of saturable absorption, and reverse saturable absorption under certain conditions. Implying that these dyes may have a potential role in applications of all optical switching devices. We suggest the use of pulsed laser for further investigation of optical limiting action.

Index Terms-Nonlinear optics, Z-scan.

I. INTRODUCTION

Recently, research on materials that exhibit third-order nonlinear properties has increased substantially for their applications in optical limiting [1], and all-optical switching devices [2]. Third-order nonlinear processes include two-photon absorption, self-phase modulation, self-focusing, and self-defocusing effects [3].

Natural organic dyes have been intensively investigated as nonlinear optical materials including saffron [4], curcumin [5],

and hibiscus [6]. However, the question of whether commercial food dyes exhibit nonlinear properties remains unclear.

One simple approach to simultaneously measure the non-linear refractive index and the nonlinear absorption coefficient is called the Z-scan technique. Formalized by Sheik-Bahae *et al* [7]. In this study, we examined the nonlinear refractive index n_2 and nonlinear absorption coefficient β of yellow food coloring (Tartrazine-Carmoisine solution) to determine the third-order nonlinear susceptibility $\chi^{(3)}$.

To measure n_2 and β we subjected a 1 mm sample to an Argon laser $\lambda = 514$ nm, focused by a biconvex lens. This creates a variable beam intensity across the optical path of the laser. Allowing the samples to reveal nonlinear refraction and absorption.

Our results indicate that commercial yellow food dyes has a negative nonlinear refractive index n_2 attributed to self-defocusing. Moreover, we report the observation of saturable absorption, and reverse saturable absorption under certain conditions. Implying that these dyes may have a role in applications of optical switching.

II. BACKGROUND

In linear optics, low-intensity light interacts with matter without changing its optical properties, and include processes such as transmission, reflection, superposition, and birefringence [3] [8]. Conventional light sources are incoherent, non-monochromatic, and have insufficient intensities to cause any change in the optical properties of matter.

Following the invention of the first laser in 1960 [9], applications of lasers grew widely in science, medicine, and manufacturing. A basic laser consists of a gain medium, that causes the amplification of light, a cavity that shapes the geometry of mirrors in which light resonates, and a pumping system that supplies the required energy for lasing [10].

Furthermore, lasers accelerated the progress in photonics by expanding the range of applications. Nonlinear optics, a branch of photonics studies the processes arising from changes of the optical properties of material caused by a high-intensity light source. Lasers being sources of monochromatic, coherent, and collimated light were the only sources that provide sufficient intensity to modify the optical properties of material [11].

Historically, developing a laser with gain medium to generate a particular frequency of light was not straightforward. However, frequency conversion was an easier task to achieve. This was done by dye lasers and nonlinear crystals. It was demonstrated that light twice the frequency of the incident frequency can be achieved by second-harmonic generation [12].

A. Light Matter Interaction

In a classical point of view, an incident light wave on a neutral material induces tiny dipole moments. The positively charged nucleus will move slightly in the direction of the electric filed, while the electron cloud will move in the opposite direction. As a consequence, an equilibrium point will be reached after oscillation, leaving the atom polarized. The density of dipole moments or the dipole moments per unit volume is defined to be the polarization **P** [13].

1) The Linear Medium: Oscillations in a linear medium due to a low-intensity electric field are fairly small. Therefore, the polarization **P** due to an electric field **E** can be described as

$$\tilde{\mathbf{P}}(t) = \epsilon_0 \chi^{(1)} \tilde{\mathbf{E}}(t) \tag{1}$$

where $\chi^{(1)}$ is the linear susceptibility, and ϵ_0 is permittivity of free space, the tilde ($\tilde{}$) denotes to a quantity that varies rapidly in time. This equation represents linear optics, where the intensity of light does not play a role in the optical properties of light [3].

2) The Nonlinear Medium: As the intensity of the electric field increases, the strict proportionality between the electric field and the polarization begins to fail. The heavy nucleus and the tightly bound inner-shell electrons are unable to oscillate at the frequency of the incident electric field. Hence, the outershell electrons are accountable for the polarization. This is better described by generalizing Equation 1 as

$$\tilde{\mathbf{P}}(t) = \epsilon_0 [\chi^{(1)} \tilde{\mathbf{E}}(t) + \chi^{(2)} \tilde{\mathbf{E}}^2(t) + \chi^{(3)} \tilde{\mathbf{E}}^3(t) + \cdots]$$
 (2)

where $\chi^{(2)}$ and $\chi^{(3)}$ are the second- and third-order nonlinear susceptibilities, respectively. The second-order susceptibility $\chi^{(2)}$ is responsible for phenomena including second-harmonic, sum difference-frequency, and difference-frequency generation. To study optical susceptibilities $\chi^{(2)}$ and $\chi^{(3)}$ it is recommenced to stay away from extreme laser intensities to limit higher orders of non-linearity such as $\chi^{(5)}$ or damaging the sample.

3) Third-Order Susceptibility: The third-order susceptibility $\chi^{(3)}$ is manifested in the nonlinear refractive index as self-actions including self-focusing, self-defocusing, self-phase modulation and beam fanning. In addition, $\chi^{(3)}$ is manifested in the nonlinear absorption as two-photon absorption, multiphoton absorption, saturable absorption, and reverse saturable absorption. The nonlinear refractive index can be described as [11]

$$n(I) = n_0 + n_2 I \tag{3}$$

where n_0 is the linear refractive index, I is the intensity of incident field, and n_2 is the nonlinear refractive index which is dependent on the incident intensity I. The nonlinear absorption can be described as [3]

$$\alpha(I) = \alpha_0 + \beta I \tag{4}$$

where α_0 is the linear absorption coefficient, and β is the nonlinear absorption coefficient. Together n_2 and β can determine the magnitude of $\chi^{(3)}$ expressed in electrostatic units (esu) through the equations

$$\operatorname{Re}\{\chi^{(3)}\}(esu) = (\frac{\epsilon_0 c^2}{10^4 \pi}) n_0^2 n_2 \ (\frac{cm^2}{W}) \tag{5}$$

$$Im\{\chi^{(3)}\}(esu) = (\frac{\epsilon_0 c^2}{4 \times 10^2 \pi^2}) n_0^2 \lambda \beta \ (\frac{cm^2}{W})$$
 (6)

$$|\chi^{(3)}| = \sqrt{(\text{Re}\{\chi^{(3)}\})^2 + (\text{Im}\{\chi^{(3)}\})^2}$$
 (7)

where c is the speed of light in a vacuum, and λ is the wavelength of the incident wave.

B. The Z-scan technique

The z-scan technique is a simple experimental approach for simultaneously measuring the nonlinear refractive index n_2 and the nonlinear absorption coefficient β . Formalized by by Sheik-Bahae $et\ al\ [7]$. The main principle is to focus a single laser beam using a biconvex lens. Thus, creating a varying intensity along the optical path (z-axis) of the laser beam. The sample is then moved using a computer controlled translation stage from a position -z to +z, where z=0 is the focus of the lens. Subsequently, the transmission is measured using a detector and the data is recorded in a computer. The geometry of the detector's aperture determines which nonlinear property is measured. A closed aperture configuration measures the nonlinear refractive index n_2 , while an open aperture configuration measures the nonlinear absorption coefficient β .

C. Z-scan Theoretical Analysis

The incident laser beam on the sample is assumed to have a TEM_{00} Gaussian profile with radius w_0 traveling in the +z direction expressed as [7]

$$E(z,r,t) = E_0(t) \frac{w_0}{w(z)} \exp(-\frac{r^2}{w(z)} - \frac{ikr^2}{2R(z)}) \exp(-\phi(z,t))$$
(8)

where $w(z)=w_0\sqrt{1+(z/z_R)},\ R(z)=z(1+z_R^2/z^2)$ is the radius of curvature of the wavefront, $z_R=\pi w_0^2/\lambda$ is the Rayleigh length, k is the wave vector, k is the laser wavelength, and k is Gouy's phase. Now we are interested in calculating changes in the phase k0 by applying the slowly varying envelope approximation (SVEA), and assuming the sample length is small so that changes in the beam diameter due to diffraction and nonlinear refraction can be neglected. This is described by

$$\frac{d\Delta\phi}{dz'} = n(I)k\tag{9}$$

$$\frac{dI}{dz'} = -\alpha(I)I\tag{10}$$

where z' is the propagation depth in the sample. Equations 9 and 10 can be solved and define the on-axis phase-shift due to nonlinear refraction $\Delta\Phi_0$ expressed as [7]

$$\Delta\Phi_0 = kn_2 I_0 L_{eff} \tag{11}$$

In addition, the on-axis phase shift due to nonlinear absorption $\Delta\Psi_0$ is

$$\Delta\Psi_0 = \frac{I_0 L_{eff}}{2\sqrt{2}}\beta\tag{12}$$

where $k=2\pi/\lambda$ is the wave vector, I_0 is the intensity of the laser beam at the focus (z=0), and L_{eff} is the effective thickness of the sample and given by

$$I_0 = \frac{2P_0}{\pi w_0^2} \tag{13}$$

$$L_{eff} = \frac{1 - \exp(-\alpha_0 L)}{\alpha_0} \tag{14}$$

where P_0 is input laser power, w_0 is the waist of the laser, α_0 is the linear absorbance coefficient, and L is the thickness of the sample.

The linear absorbance coefficient α_0 can then be calculated using the definition of absorbance A according to $A=-\log T$ [14], where T is the transmittance equal to the ratio between the input irradiance and the output irradiance, $T=\exp(-\alpha_0 L)$, and L is the length of the sample. Therefore α_0 is expressed as

$$\alpha_0 = A \frac{\ln 10}{L} \tag{15}$$

1) Gaussian Decomposition Model: After passing through the sample, the complex electric field has nonlinear phase distortion and expressed as [7]

$$E_e(r, z, t) = E(r, z, t) \exp(-\frac{\alpha L}{2}) \exp(i\Delta\phi(z, r, t)) \quad (16)$$

The phase term $\exp(i\Delta\phi(z,r,t))$ is then decomposed into a summation of Gaussian beams by Taylor series expansion, this is knows as "Gaussian decomposition". To get an expression for the power through an aperture, the electric field expression containing the decomposed phase term E_a is integrated along the radius of the aperture

$$P_T(\Delta\Phi(t)) = c\epsilon_0 \pi \int_0^{r_a} |E_a(r,t)|^2 r dr$$
 (17)

Thence, the normalized Z-scan transmittance T(z) can be determined by

$$T(z) = \frac{\int_{-\infty}^{\infty} P_T(\Delta\Phi(t))dt}{S\int_{-\infty}^{\infty} P_i(t)dt}$$
(18)

where $S=1-\exp(-2r_a^2/w_a^2)$ is the aperture linear transmittance, $P_i(t)=\pi w_0^2 I_0(t)/2$ is the instantaneous input power through the sample.

The Gaussian decomposition model assumes that nonlinear absorption is negligible, and nonlinearities are purely due to nonlinear refraction. Resulting in a geometry-independent expression that displays peak-valley symmetry for the normalized transmittance of the form

$$T(z) = 1 + \frac{4x\Delta\Phi_0}{(x^2 + 9)(x^2 + 1)}$$
(19)

where $x=z/z_R$, and $z_R=\pi w_0^2/\lambda$ is the Rayleigh length. Consequently, Equation 19 can be fitted with closed-aperture experimental data to deduce $\Delta\Phi_0$. Furthermore, the difference between the peak and valley of the normalized transmittance $\Delta T_{p-v}=T_p-T_v$, is found to be proportional to $\Delta\Phi_0$ for $(S\simeq 0)$ [7]

$$\Delta T_{p-v} \simeq 0.406 |\Delta \Phi_0| \tag{20}$$

When nonlinear absorption is more pronounced openaperture experimental data can be fitted with [3]

$$T(z) = 1 - \frac{\Delta\Psi_0}{(x^2 + 1)} \tag{21}$$

Z-scans of materials that exhibit both nonlinear refraction and nonlinear absorption cannot be adequately fitted by Equation 19. In that case the normalized transmittance shows an asymmetric peak-valley and given by [15]

$$T(z) = 1 + \frac{4x\Delta\Phi_0}{(x^2+9)(x^2+1)} - \frac{2(x^2+3)\Delta\Psi_0}{(x^2+9)(x^2+1)}$$
 (22)

2) Thermal Lens Model: Oftentimes, using a continuous wave laser results in the local heating of the sample. This is due to a large single-photon absorption. The normalized transmittance peak is sharply enhanced while the valley is greatly depressed. This indicates a high single-photon absorption. The normalized transmission can be given by [3] [15]

$$T(z) = \left[1 + \Delta\Phi_0 \frac{2x}{(x^2 + 1)} + \Delta\Phi_0^2 \frac{2x}{(x^2 + 1)}\right]^{-1}$$
 (23)

III. MATERIALS AND METHODS

A. Experimental technique

NATCO yellow food coloring, is primarily composed of Tartazine E102 and Carmosine E122, dissolved in water with traces of acetic acid. Tartazine and Carmosine are widely used as commercial food dye that are also found cosmetics, medication, and inks. For the purpose of this study, the yellow dyes was diluted using distilled water to achieve three concentrations in ratios as dye: distilled water, namely 1 ml: 21 ml, 1 ml: 15 ml, and 1 ml: 7.5 ml.

To obtain the linear absorbance spectrum, the three samples were prepared to fill 10 mm quartz cuvettes. The dual beam spectrometer Shimadzu UV-VIS NIR (UV-3600) was used. Absorbance values were recorded from a wavelength of

 $\lambda=480$ nm to $\lambda=600$ nm. A reference cuvette of the same size filled with distilled water was placed in each scan.

The experimental approach followed in this study is the Z-scan technique [7]. The three concentrations were placed in 1 mm quartz cuvette mounted on a computer controlled translating stage. The sample is then moved through the optical path (z-axis) of a 2214-25ML air cooled argon laser at a wavelength $\lambda=514$ nm. The laser beam is focused by a biconvex lens with a focal length of 10 cm, which marks the origin of the z-axis (z=0).

The sample starts from a position $z=-30 \mathrm{mm}$ passing through the focus z=0 to stop at $z=30 \mathrm{mm}$. The transmittance was recorded in the far field $(z>>z_R)$ using a closed-aperture configuration to determine the nonlinear refractive index n_2 , illustrated in Figure 1. In addition, the transmittance was separately recorded using an open-aperture configuration to determine the nonlinear absorption coefficient β , as illustrated in Figure 2. Signals from the detector are processed by Phywe Cobra3 Unit, to be displayed in a computer using Phywe "measure" software. The acquired experimental data are then fitted minimizing square loss using Python and the scipy.optimize.curve_fit function.

In some cases, where the intensity of the laser beam is high enough to saturate the detector, a set of polarizers and analyzers are used, to decrease the intensity.

In addition, the fluorescence spectrum was acquired by shining the laser through a sample of concentration 1 ml:7.5 ml placed in a 10 mm cuvette. The recorded intensity was between a wavelength of $\lambda=400$ nm and $\lambda=780$ nm.

1) Closed Aperture Configuration: To measure n_2 and determine $\text{Re}\{\chi^{(3)}\}$, the sample is translated through the optical path of the laser. Placing an aperture before the detector allowing only a portion of the transmitted light to hit the detector as illustrated in Figure 1.

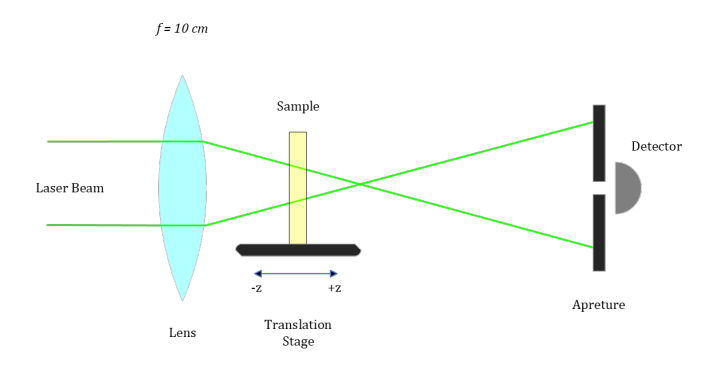


Fig. 1. Closed Aperture Setup

2) Open Aperture Configuration: To measure β and determine $\mathrm{Im}\{\chi^{(3)}\}$, the sample is translated through the optical path of the laser. Allowing all the light to hit the detector. The same closed-aperture detector was used with the addition of a focusing lens to collect the light through the small aperture. This is shown in Figure 2.

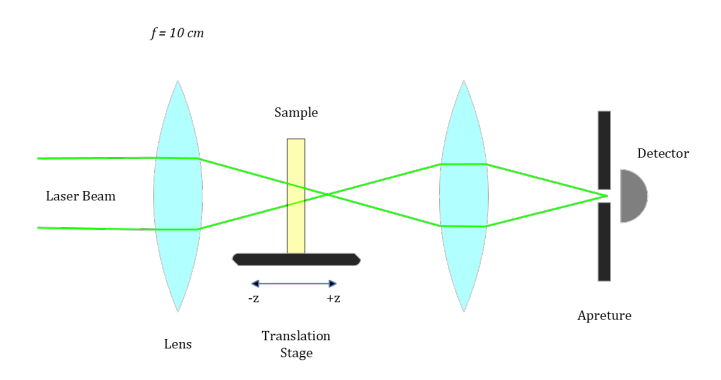


Fig. 2. Open Aperture Setup

3) Optical Limiting Configuration: The setup shown in Figure 3 was followed to investigate if the samples possess optical limiting behaviour. The sample is placed about the focal point of the focusing lens, ideally in the position of the valley of the Z-scan to exploit nonlinear absorption. A laser power-meter detector is placed before entering the sample to record the input power. After that, corresponding measurements of the output power are recorded by placing the detector after the sample.

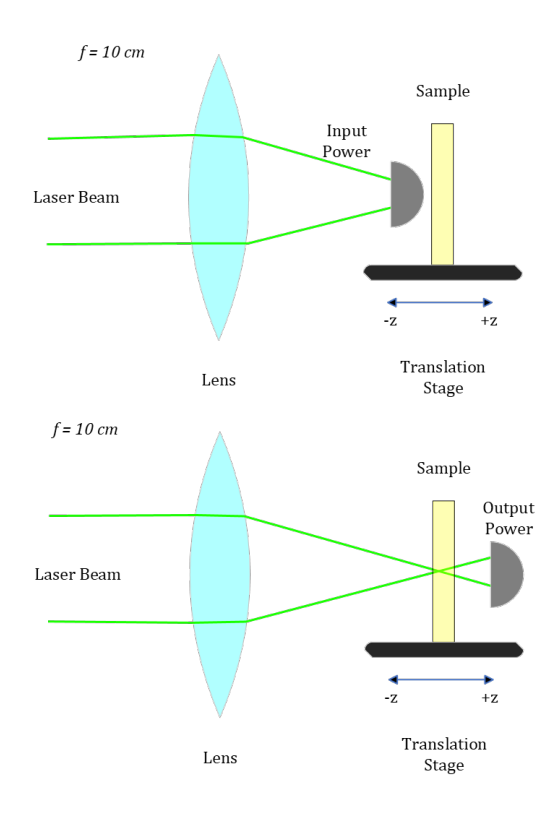


Fig. 3. Optical Limiting Setup

Figure 4 shows the linear absorbance of three samples of the yellow dye, measured for three concentrations, namely 1 ml : 21 ml, 1 ml : 15 ml, and 1 ml : 7.5 ml (dye : distilled water). When $\lambda=514$ nm the absorbance was found to be 0.553, 0.749, and 1.335 respectively . The values were measured in absorbance units. As shown the absorbance increases rapidly with decreasing wavelengths below $\lambda=500$ nm. The linear absorption coefficient α_0 was determined from these values using Equation 15 and tabulated with the corresponding effective length L_{eff} in Table I.

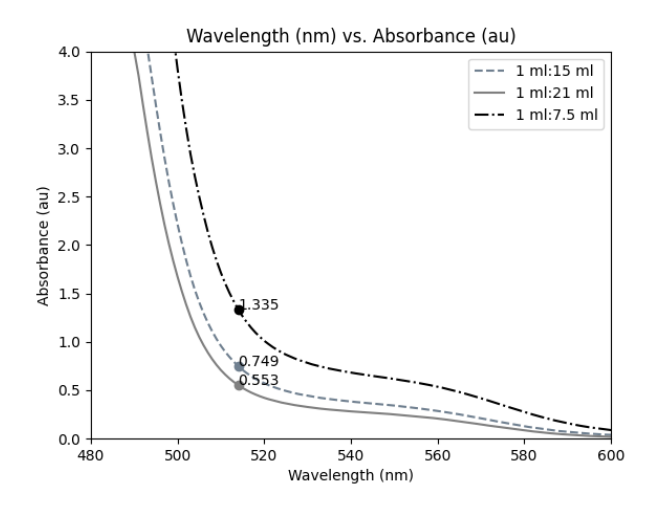


Fig. 4. Linear absorbance of three concentrations of the yellow dye solution. The indicated points are the absorbance values at $\lambda = 514$ nm.

TABLE I
LINEAR ABSORBANCE AND EFFECTIVE LENGTH AT DIFFERENT
CONCENTRATIONS

Concentration	$\alpha_0(\mathrm{m}^{-1})$	$L_{eff}(\mathrm{mm})$
1 ml: 21 ml	127.3	0.939
1 ml: 15 ml	172.5	0.919
1 ml: 7.5 ml	307.4	0.860

Figure 5 shows the fluorescence spectrum of the of the sample with concentration 1 ml:7.5 ml. The measured intensity is recorded in arbitrary units. The fluorescence peaks at a wavelength around $\lambda=630$ nm.

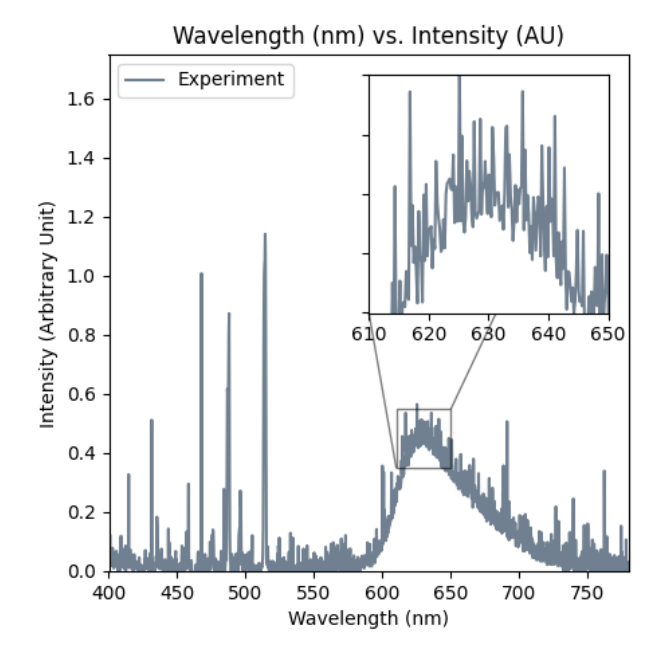


Fig. 5. Fluorescence spectrum of sample with concentration 1 ml:7.5 ml

To investigate optical limiting behaviour, the experimental setup illustrated in Figure 3 was followed to measure the input power before entering the sample and just after exiting. The relationship appears to be linear when the excitation power is less than 2.5 mW as evident in Figure 6.

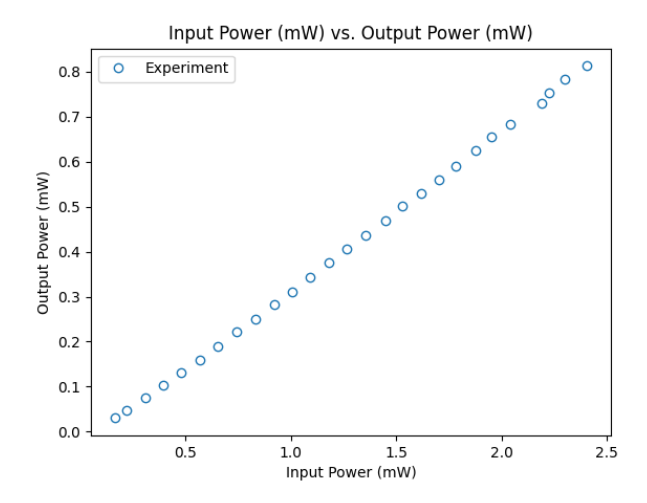


Fig. 6. Input vs. output power of sample with concentration 1 ml:7.5 ml

A. Gaussian Decomposition Fitting

The Gaussian decomposition model is fitted with closed-aperture experimental data minimizing square loss. Figures 7 through 15 illustrate the closed aperture normalized transmittance of three concentrations at three power levels. Equation 19 appearing as blue dashed lines labeled "Not accounting absorption", and Equation 22 appearing as a solid red line labeled "Accounting absorption".

The first observation is that the nonlinear refractive index is negative for all. This is deduced by noting that the peak of transmittance is located at z<0 and the valley is located at z>0.

Using the obtained fitting parameters $\Delta\Phi_0$ and $\Delta\Psi_0$, the nonlinear refractive index n_2 is evaluated using Equation, 11, while the nonlinear absorption coefficient β is evaluated using Equation 12. From the evaluated n_2 and β , the third-order susceptibility $\chi^{(3)}$ is calculated using Equations 5, 6, and 7.

Each subsection contains the closed-aperture Z-scan result of each concentration, at excitation powers 0.500 mW, 1.000 mW, and 1.500 mW. Followed by tabulated values of $\Delta\Phi_0$, $\Delta\Psi_0$, ΔT_{p-v} , n_2 , β , $\mathrm{Re}\{\chi^{(3)}\}$, $\mathrm{Im}\{\chi^{(3)}\}$, and $\chi^{(3)}$.

1) Concentration 1 ml: 21 ml: As seen in figure 7, the normalized transmittance shows a symmetrical peak-valley, and both equations (19 and 22) fit the experimental data adequately. However, increasing the excitation power results in Equation 22 having a better fit, as illustrated in Figures 8 and 9. This is suggested by the increase in $\Delta\Psi_0$ from -0.014 to -0.052 listed in Table II.

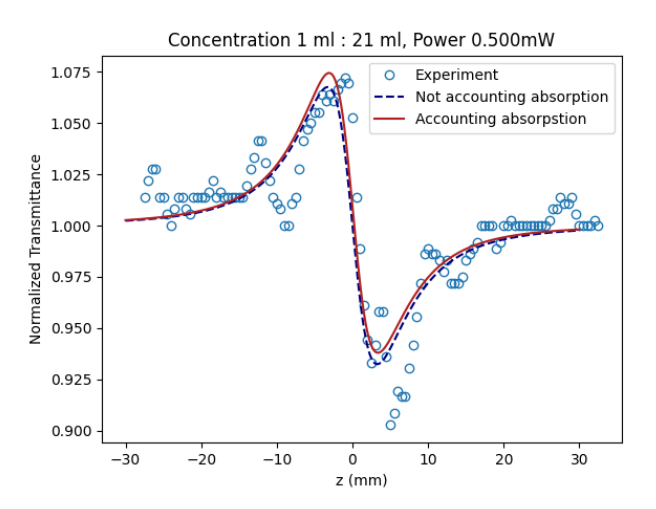


Fig. 7. Normalized transmittance for closed aperture Z-scan of concentration 1 ml:21 ml and power 0.500 mW, fitted with the Gaussian decomposition model, accounting absorption compared with not accounting absorption.

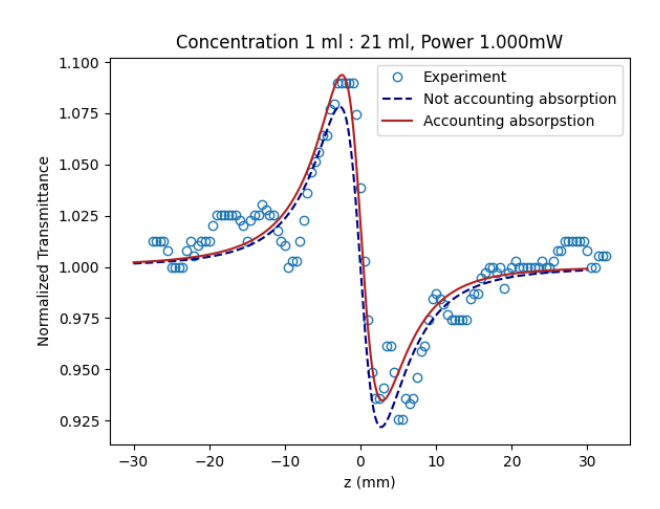


Fig. 8. Normalized transmittance for closed aperture Z-scan of concentration 1 ml:21 ml and power 1.000 mW, fitted with the Gaussian decomposition model, accounting absorption compared with not accounting absorption.

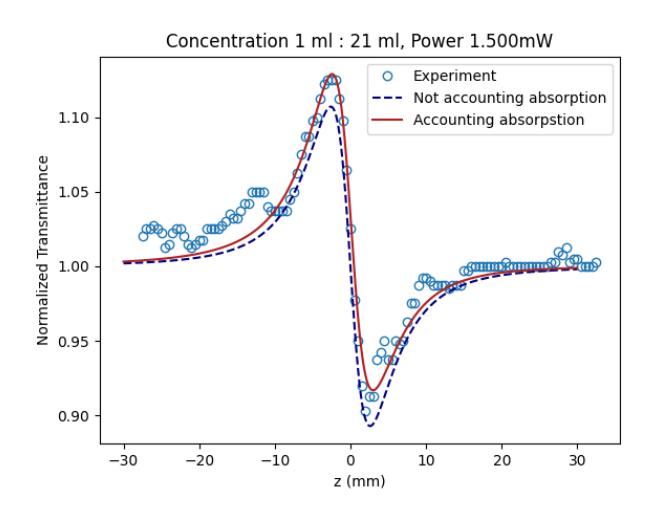


Fig. 9. Normalized transmittance for closed aperture Z-scan of concentration 1 ml:21 ml and power 1.500 mW, fitted with the Gaussian decomposition model, accounting absorption compared with not accounting absorption.

TABLE II FITTING PARAMETERS FOR A SAMPLE OF CONCENTRATION 1 ML : 21 ML $\,$

Power(mW)	$\Delta\Phi_0$	$\Delta\Psi_0$	ΔT_{p-v}
0.500	-0.336	-0.014	0.135
1.000	-0.390	-0.032	0.156
1.500	-0.519	-0.052	0.215

 $TABLE\ III \\ Nonlinear\ refraction\ index\ and\ absorption\ coefficient\ at\ different\ powers\ for\ a\ sample\ of\ concentration\ 1\ mL:\ 21\ mL$

Power(mW)	$n_2 \times 10^{-14} (\text{m}^2/\text{W})$	$\beta \times 10^{-8} (\text{m/W})$
0.500	-3.93	-5.69
1.000	-2.28	-6.53
1.500	-2.03	-7.03

TABLE IV
IMAGINARY, REAL AND MAGNITUDE OF THIRD-ORDER NONLINEAR
SUSCEPTIBILITY AT DIFFERENT POWERS FOR A SAMPLE OF
CONCENTRATION 1 ML: 21 ML

Power(mW)	$Re\{\chi^{(3)}\} \times 10^{-8}(esu)$	$Im\{\chi^{(3)}\} \times 10^{-9}(esu)$	$ \chi^{(3)} \times 10^{-8} (esu)$
0.500	-1.77	1.05	1.77
1.000	-1.03	1.20	1.034
1.500	-0.913	1.29	0.922

2) Concentration 1 ml: 15 ml: As shown in Figures 10 and 11, increasing the concentration of the sample leads to an asymmetric normalized transmittance, enhancing the peak and depressing the valley at a low excitation power of 0.500 mW and 1.000 mW. In that case, Equation 22 has a better fit experimental data than Equation 19. Nevertheless, at higher excitation power the normalized transmittance curve approaches symmetry as depicted in figure 12.

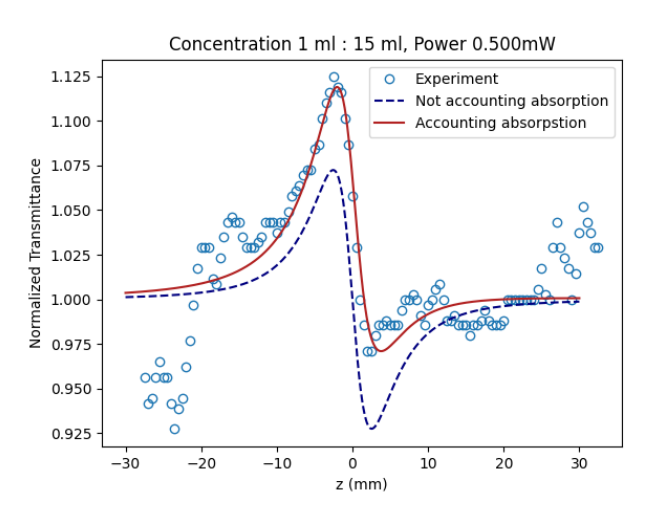


Fig. 10. Normalized transmittance for closed aperture Z-scan of concentration 1 ml:15 ml and power 0.500 mW, fitted with the Gaussian decomposition model, accounting absorption compared with not accounting absorption.

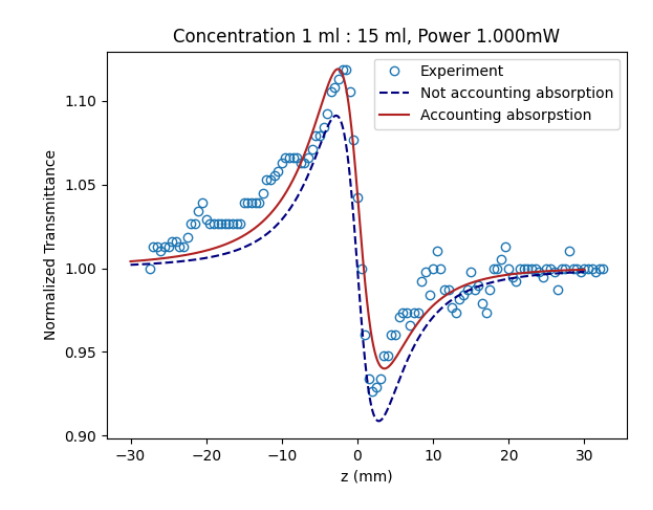


Fig. 11. Normalized transmittance for closed aperture Z-scan of concentration 1 ml:15 ml and power 1.000 mW, fitted with the Gaussian decomposition model, accounting absorption compared with not accounting absorption.

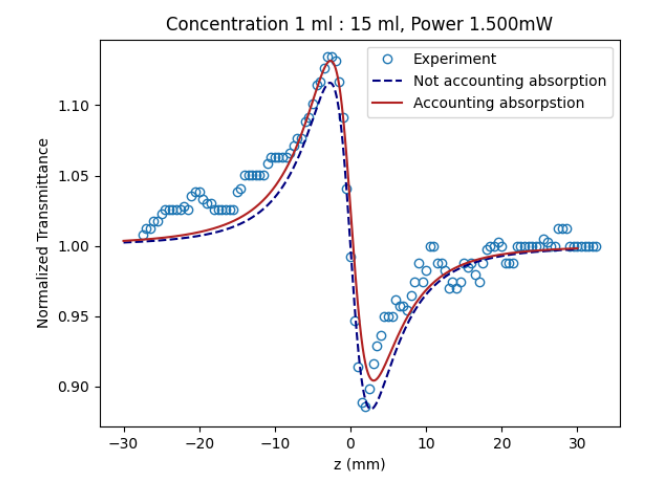


Fig. 12. Normalized transmittance for closed aperture Z-scan of concentration 1 ml:15 ml and power 1.500 mW, fitted with the Gaussian decomposition model, accounting absorption compared with not accounting absorption.

TABLE V FITTING PARAMETERS FOR A SAMPLE OF CONCENTRATION 1 ML : 15 ML $\,$

Power(mW)	$\Delta\Phi_0$	$\Delta \Psi_0$	ΔT_{p-v}
0.500	-0.343	-0.102	0.145
1.000	-0.434	-0.067	0.183
1.500	-0.558	-0.041	0.232

 $TABLE\ VI \\ Nonlinear\ refraction\ index\ and\ absorption\ coefficient\ at\ different\ powers\ for\ a\ sample\ of\ concentration\ 1\ mL:15\ mL$

Power(mW)	$n_2 \times 10^{-14} (\text{m}^2/\text{W})$	$\beta \times 10^{-7} (\text{m/W})$
0.500	-4.11	-4.24
1.000	-2.60	-1.39
1.500	-2.23	-0.560

TABLE VII
IMAGINARY, REAL AND MAGNITUDE OF THIRD-ORDER NONLINEAR
SUSCEPTIBILITY AT DIFFERENT POWERS FOR A SAMPLE OF
CONCENTRATION 1 ML: 15 ML

Power(mW)	$Re\{\chi^{(3)}\} \times 10^{-8}(esu)$	$Im\{\chi^{(3)}\} \times 10^{-9}(esu)$	$ \chi^{(3)} \times 10^{-8} (esu)$
0.500	-1.85	7.80	2.01
1.000	-1.17	2.56	1.20
1.500	-1.00	1.03	1.01

3) Concentration 1 ml: 7.5 ml: Figures 13 and 14 show a symmetrical normalized transmittance. This is suggested from the low values of $\Delta\Psi_0$ which are -0.028, and 0.048 at excitation powers 0.5 mW, and 1.000 mW respectively. However, $\Delta\Psi_0$ changes from a negative to a positive value, as well as a sudden increase in $\Delta\Psi_0$ to be 0.218 when the excitation power is 1.500 mW. The positive value of $\Delta\Psi_0$ is leads to an asymmetrical normalized transmittance with a suppressed peak and a deeper valley.

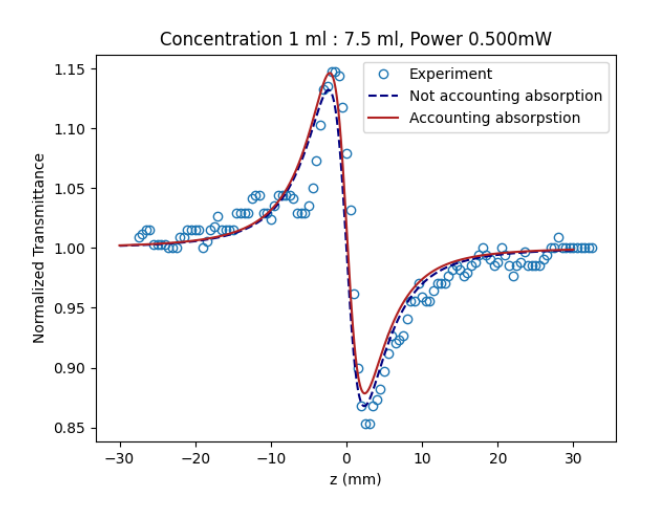


Fig. 13. Normalized transmittance for closed aperture Z-scan of concentration 1 ml:7.5 ml and power 0.500 mW, fitted with the Gaussian decomposition model, accounting absorption compared with not accounting absorption.

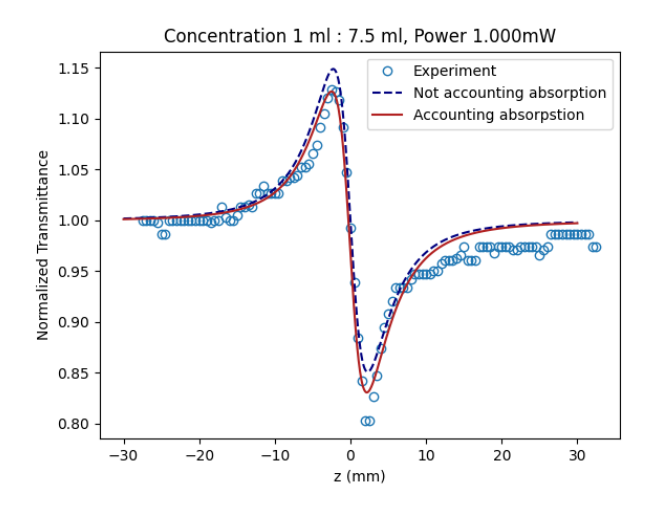


Fig. 14. Normalized transmittance for closed aperture Z-scan of concentration 1 ml:7.5 ml and power 1.000 mW, fitted with the Gaussian decomposition model, accounting absorption compared with not accounting absorption.

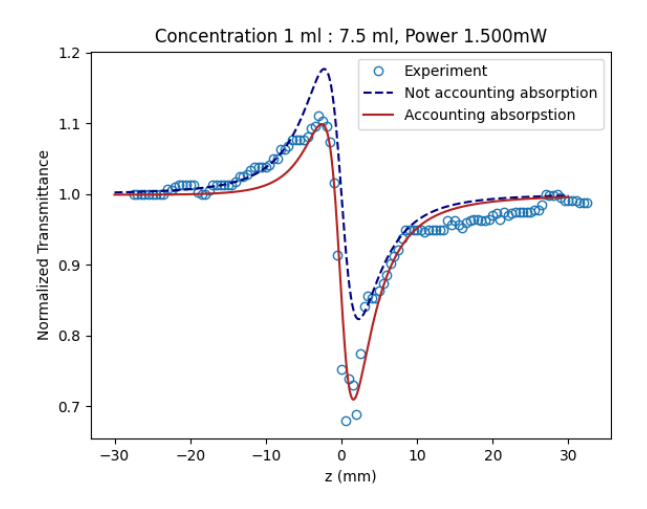


Fig. 15. Normalized transmittance for closed aperture Z-scan of concentration 1 ml:7.5 ml and power 1.500 mW, fitted with the Gaussian decomposition model, accounting absorption compared with not accounting absorption.

Power(mW)	$\Delta\Phi_0$	$\Delta \Psi_0$	ΔT_{p-v}
0.500	-0.659	-0.028	0.264
1.000	-0.727	0.048	0.298
1.500	-0.925	0.218	0.298

 $TABLE\ IX \\ Nonlinear\ refraction\ index\ and\ absorption\ coefficient\ at\ different\ powers\ for\ a\ sample\ of\ concentration\ 1\ mL: 7.5\ mL$

Power(mW)	$n_2 \times 10^{-14} (\text{m}^2/\text{W})$	$\beta \times 10^{-7} (\text{m/W})$
0.500	-8.41	-1.24
1.000	-4.64	1.06
1.500	-3.94	3.21

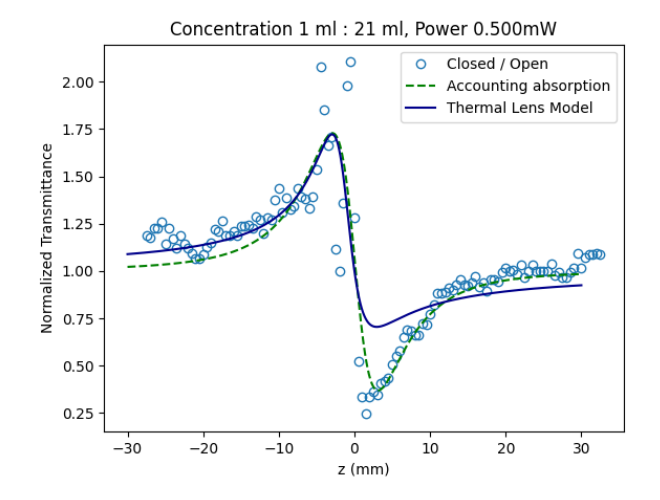


Fig. 16. Normalized transmittance for closed/open aperture Z-scan of concentration 1 ml:21 ml and power 0.500 mW, fitted with the Gaussian decomposition model and the thermal lens model

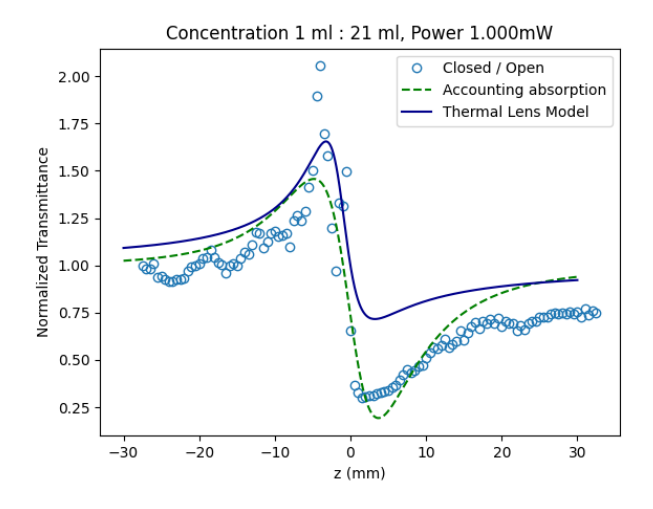


Fig. 17. Normalized transmittance for closed/open aperture Z-scan of concentration 1 ml:21 ml and power 1.000 mW, fitted with the Gaussian decomposition model and the thermal lens model

TABLE X
IMAGINARY, REAL AND MAGNITUDE OF THIRD-ORDER NONLINEAR
SUSCEPTIBILITY AT DIFFERENT POWERS FOR A SAMPLE OF
CONCENTRATION 1 ML: 7.5 ML

Power(mW)	$Re\{\chi^{(3)}\} \times 10^{-8}(esu)$	$Im\{\chi^{(3)}\} \times 10^{-9}(esu)$	$ \chi^{(3)} \times 10^{-8} (esu)$
0.500	-3.79	2.27	3.79
1.000	-2.09	-1.95	2.10
1.500	-1.77	-5.91	1.87

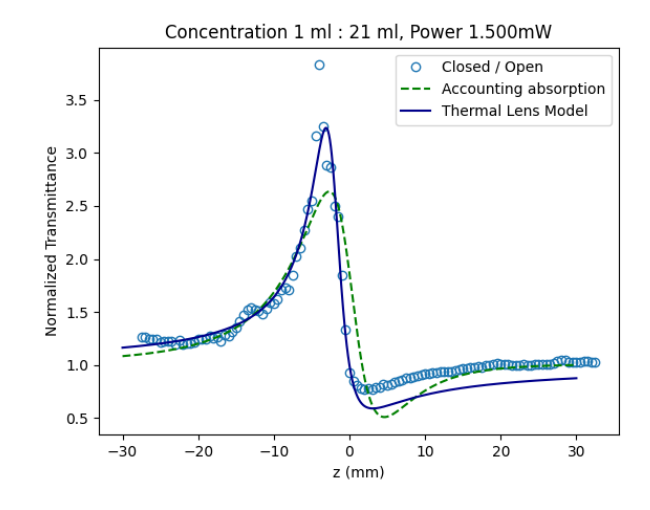


Fig. 18. Normalized transmittance for closed/open aperture Z-scan of concentration 1 ml:21 ml and power 1.500 mW, fitted with the Gaussian decomposition model and the thermal lens model

B. Thermal Lens Model Fitting

The Thermal lens model is fitted with closed-aperture experimental divided by the corresponding open-aperture data, data minimizing square loss. Figures 16 through 24 illustrate the normalized transmittance of the same three concentrations at three power levels. The Gaussian decomposition Equation 19 appearing as green dashed lines labeled "Accounting absorption", and Equation 23 appearing as a solid blue line labeled "Thermal Lens Model". A similar procedure to the Gaussian decomposition fitting has been followed to calculate the nonlinear optical parameters.

 $\begin{tabular}{ll} TABLE~XI\\ FITTING~PARAMETERS~FOR~CLOSED/OPEN~APERTURE~DATA~1~ML:~21~ML \end{tabular}$

Power(mW)	$\Delta\Phi_0$	$\Delta \Psi_0$	ΔT_{p-v}
0.500	-3.34	-0.11	1.36
1.000	-3.080	0.40	1.26
1.500	-5.00	-1.30	2.12

TABLE XII

NONLINEAR REFRACTION INDEX AND ABSORPTION COEFFICIENT AT
DIFFERENT POWERS FOR A SAMPLE OF CONCENTRATION 1 ML: 21 ML

Power(mW)	$n_2 \times 10^{-13} (\text{m}^2/\text{W})$	$\beta \times 10^{-7} (\text{m/W})$
0.500	-3.92	-4.44
1.000	-1.80	8.03
1.500	-1.95	-17.6

TABLE XIII
IMAGINARY, REAL AND MAGNITUDE OF THIRD-ORDER NONLINEAR
SUSCEPTIBILITY AT DIFFERENT POWERS FOR A SAMPLE OF
CONCENTRATION 1 ML: 21 ML

Power(mW)	$Re\{\chi^{(3)}\} \times 10^{-8}(esu)$	$Im\{\chi^{(3)}\} \times 10^{-8}(esu)$	$ \chi^{(3)} \times 10^{-8} (esu)$
0.500	-17.6	0.817	17.6
1.000	-8.11	-1.48	8.24
1.500	-8.79	3.24	9.37

TABLE XIV THERMAL LENS MODEL FITTING PARAMETER, NONLINEAR REFRACTIVE INDEX, AND REAL PART OF SUSCEPTIBILITY FOR A SAMPLE OF CONCENTRATION 1 ML : 21 ML

Power(mW)	$\Delta\Phi_0$	$n_2 \times 10^{-13} (\text{m}^2/\text{W})$	$Re\{\chi^{(3)}\} \times 10^{-9} (esu)$	ΔT_{p-v}
0.500	0.32	3.72	16.8	1.02
1.000	0.30	1.78	8.00	0.938
1.500	0.47	1.84	8.26	2.64

1) Concentration 1 ml: 21 ml:

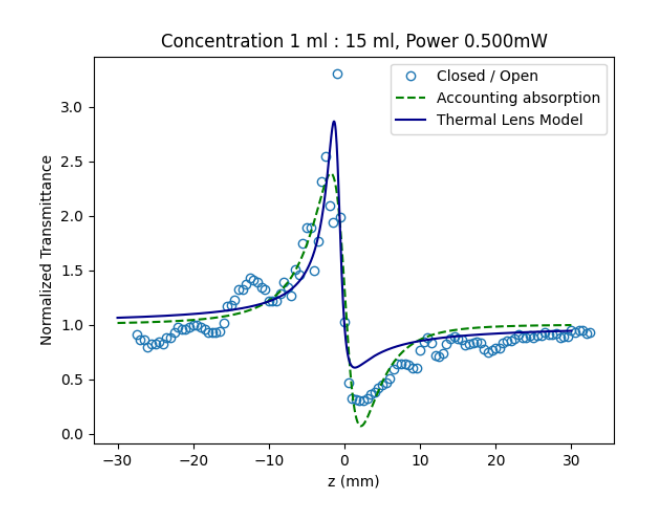


Fig. 19. Normalized transmittance for closed/open aperture Z-scan of concentration 1 ml:15 ml and power 0.500 mW, fitted with the Gaussian decomposition model and the thermal lens model

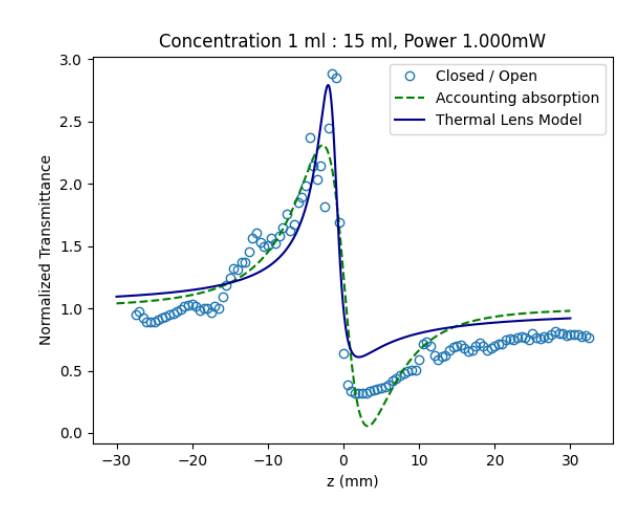


Fig. 20. Normalized transmittance for closed/open aperture Z-scan of concentration 1 ml:15 ml and power 1.000 mW, fitted with the Gaussian decomposition model and the thermal lens model

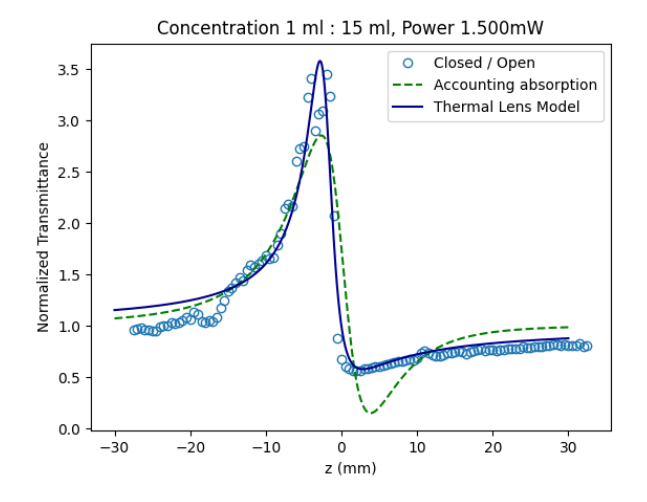


Fig. 21. Normalized transmittance for closed/open aperture Z-scan of concentration 1 ml:15 ml and power 1.500 mW, fitted with the Gaussian decomposition model and the thermal lens model

TABLE XV FITTING PARAMETERS

Power(mW)	$\Delta\Phi_0$	$\Delta \Psi_0$	ΔT_{p-v}
0.500	-5.68	-0.52	2.31
1.000	-5.53	-0.41	2.25
1.500	-5.52	-1.15	2.70

TABLE XVI
NONLINEAR REFRACTION INDEX AND ABSORPTION COEFFICIENT AT
DIFFERENT POWERS

Power(mW)	$n_2 \times 10^{-13} (\text{m}^2/\text{W})$	$\beta \times 10^{-6} (\text{m/W})$
0.500	-6.80	-2.14
1.000	-3.31	-0.854
1.500	-2.60	-1.58

TABLE XVII IMAGINARY, REAL AND MAGNITUDE OF THIRD-ORDER NONLINEAR SUSCEPTIBILITY AT DIFFERENT POWERS

Power(mW)	$Re\{\chi^{(3)}\} \times 10^{-7} (esu)$	$Im\{\chi^{(3)}\} \times 10^{-8}(esu)$	$ \chi^{(3)} \times 10^{-7} (esu)$
0.500	-3.06	3.95	3.08
1.000	-1.49	1.57	1.50
1.500	-1.17	2.91	1.21

TABLE XVIII
THERMAL LENS MODEL FITTING PARAMETER, NONLINEAR REFRACTIVE INDEX, AND REAL PART OF SUSCEPTIBILITY

Power(mW)	$\Delta\Phi_0$	$n_2 \times 10^{-14} (\text{m}^2/\text{W})$	$Re\{\chi^{(3)}\} \times 10^{-8}(esu)$	ΔT_{p-v}
0.500	0.45	5.38	2.42	2.26
1.000	0.44	2.66	1.20	2.18
1.500	0.49	1.94	0.872	3.00

2) Concentration 1 ml: 15 ml:

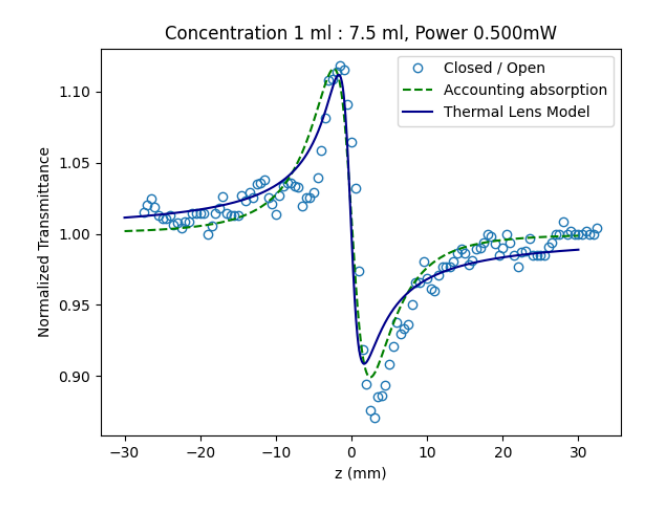


Fig. 22. Normalized transmittance for closed/open aperture Z-scan of concentration 1 ml:7.5 ml and power 0.500 mW, fitted with the Gaussian decomposition model and the thermal lens model

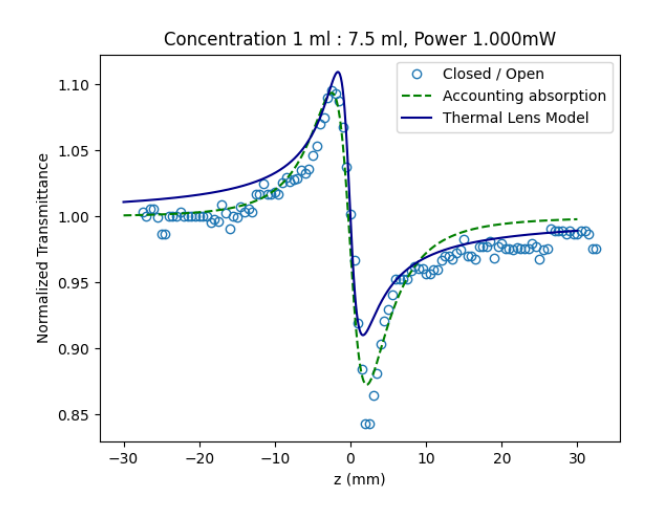


Fig. 23. Normalized transmittance for closed/open aperture Z-scan of concentration 1 ml:7.5 ml and power 1.000 mW, fitted with the Gaussian decomposition model and the thermal lens model

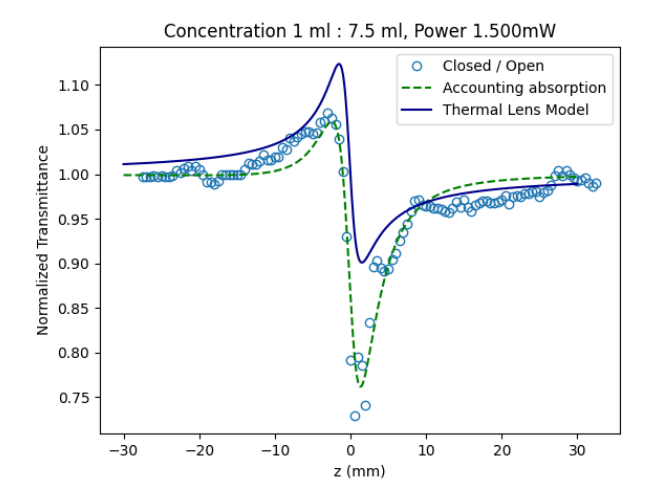


Fig. 24. Normalized transmittance for closed/open aperture Z-scan of concentration 1 ml:7.5 ml and power 1.500 mW, fitted with the Gaussian decomposition model and the thermal lens model

TABLE XIX
FITTING PARAMETERS

Power(mW)	$\Delta\Phi_0$	$\Delta \Psi_0$	ΔT_{p-v}
0.500	0.534	-0.017	0.217
1.000	-0.543	0.038	0.221
1.500	-0.690	0.204	0.297

TABLE XX
NONLINEAR REFRACTION INDEX AND ABSORPTION COEFFICIENT AT
DIFFERENT POWERS

Power(mW)	$n_2 \times 10^{-14} (\text{m}^2/\text{W})$	$\beta \times 10^{-8} (\text{m/W})$
0.500	6.82	-7.61
1.000	-3.47	-8.41
1.500	-2.94	-30.1

TABLE XXI IMAGINARY, REAL AND MAGNITUDE OF THIRD-ORDER NONLINEAR SUSCEPTIBILITY AT DIFFERENT POWERS

Power(mW)	$Re\{\chi^{(3)}\} \times 10^{-8}(esu)$	$Im\{\chi^{(3)}\} \times 10^{-9}(esu)$	$ \chi^{(3)} \times 10^{-8} (esu)$
0.500	3.07	1.40	3.07
1.000	-1.56	-1.55	1.57
1.500	-1.32	-5.53	1.43

TABLE XXII
THERMAL LENS MODEL FITTING PARAMETER, NONLINEAR REFRACTIVE INDEX, AND REAL PART OF SUSCEPTIBILITY

Power(mW)	$\Delta\Phi_0$	$n_2 \times 10^{-15} (\text{m}^2/\text{W})$	$Re\{\chi^{(3)}\} \times 10^{-9} (esu)$	ΔT_{p-v}
0.500	0.092	1.18	5.30	0.203
1.000	0.091	5.78	2.60	0.199
1.500	0.100	4.26	1.92	0.222

3) Concentration 1 ml: 7.5 ml:

C. Control

To ensure that the nonlinear behaviour presented is originating from the yellow food dye, the same experiments have been conducted using the solvent (distilled water). The closed-aperture Z-scans for the excitation powers 0.500 mW, 1.000 mW, and 1.500 mW are shown in Figures 25, 26, and 27 respectively. The Z-scans normalized transmittance showed an average and mode of approximately one, which means that most of the light is transmitted.

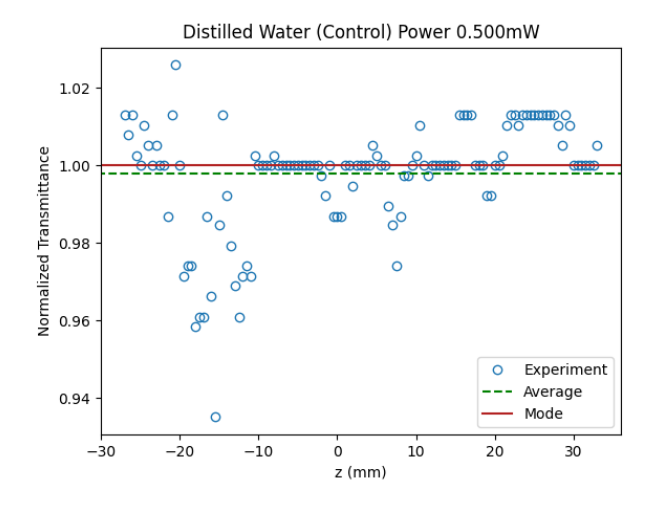


Fig. 25. Normalized transmittance for closed aperture Z-scan of distilled water at power $0.500\ mW$

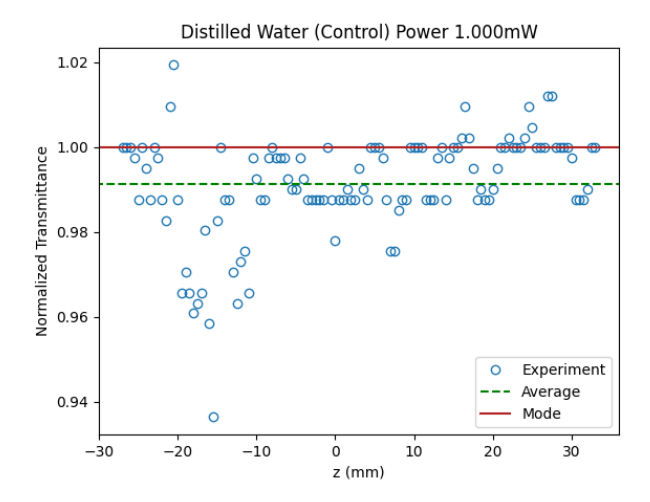


Fig. 26. Normalized transmittance for closed aperture Z-scan of distilled water at power 1.000 \mbox{mW}

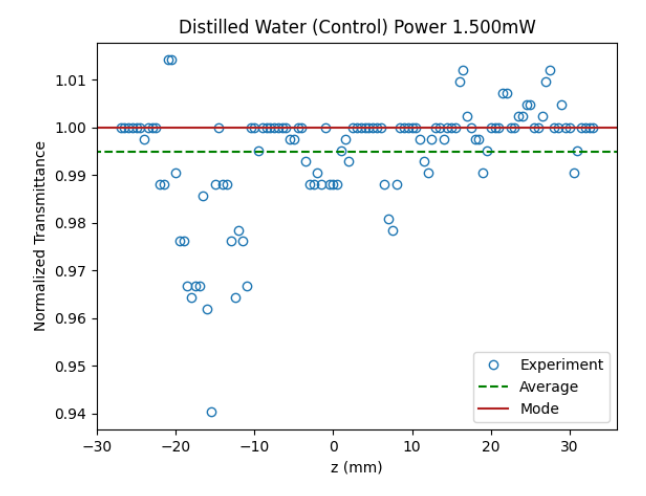


Fig. 27. Normalized transmittance for closed aperture Z-scan of distilled water at power 1.500 mW

V. DISCUSSION

Our closed-aperture Z-scan results that show symmetrical normalized transmittance have $\Delta T_{p-v}/\Delta\Phi_0\simeq 0.406$, which is in agreement with Equation 20 from literature [7]. We identified that the sign of nonlinear refractive index is negative $n_2<0$, this suggests that the samples exhibit self-defocusing [3]. Figure 28 depicts the relationship between the magnitude of nonlinear refractive index and excitation powers, the magnitude of n_2 appears to decrease with higher powers for all concentrations.

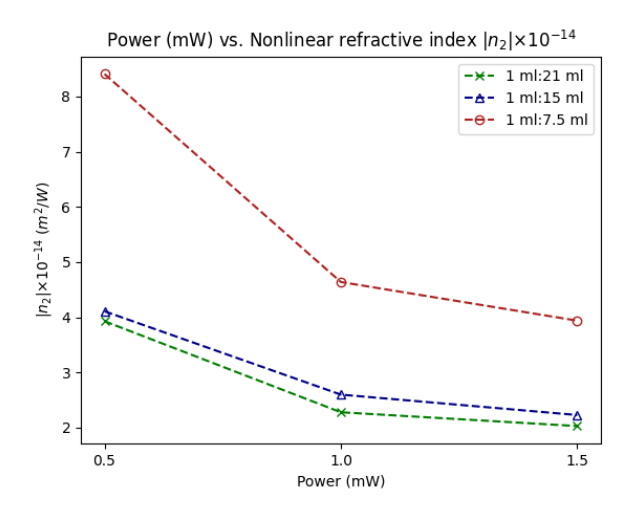


Fig. 28. Nonlinear refractive index n_2 at different excitation powers.

Our findings show at certain concentrations and excitation powers, the samples demonstrate nonlinear absorption. This is clearly evident by the asymmetric normalized transmittance curves shown in Figures 10 and 15. Figure 10 has an enhanced peak and depressed valley which indicates that the sample exhibits saturable absorption. Figure 15 has a suppressed peak and a deeper valley suggesting that the sample exhibits reverse saturable absorption or two-photon absorption. To our surprise, the value of the nonlinear absorption coefficient changes from negative to positive at a concentration of 1 ml:21 ml with increasing power. This is illustrated in Figure 29.

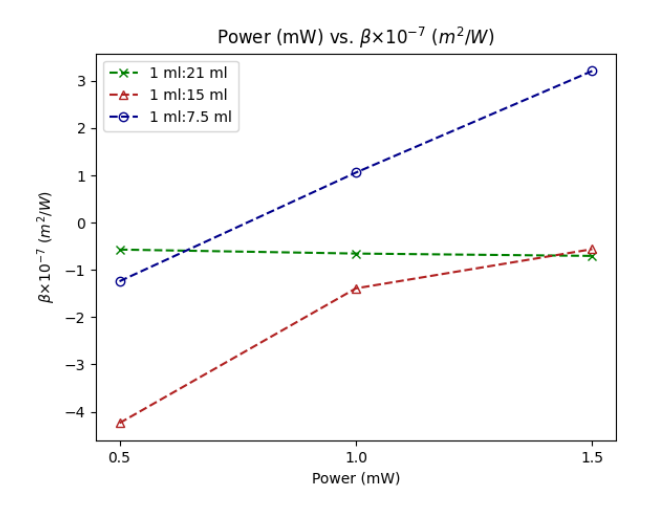


Fig. 29. Nonlinear absorption coefficient β at different excitation powers.

At a concentration 1 ml:15 ml and power 1.500 mW, the thermal lens model adequately fits the experimental data, having $\Delta T_{p-v} \approx 3.00$. It has been suggested that a $\Delta T_{p-v} > 1.7$ indicates a thermal lensing nonlinearity origin. Moreover, this is backed up by Figure 4, where the linear absorbance at $\lambda = 514$ nm is relatively high indicating single-photon absorption [3].

The relationship obtained between the input and output data shown in Figure 6 did not show any flat region. The laser used could not exceed 2.5 mW of power without overheating. Similar research on azo dyes begin to show optical limiting around an input power of 10 mW [16]. Therefore, the optical limiting behavior of yellow dye solutions remain inconclusive.

In summary, our results indicate that the samples exhibit self-defocusing, saturable absorption, and reverse saturable absorption. In addition, the results imply that yellow dyes are a promising material that show nonlinear behavior at low excitation power below 2.000 mW that could have applications in all-optical switching devices. Further experiments are needed to determine whether the samples posses optical limiting behavior.

VI. CONCLUSION

In conclusion, the linear properties of the samples were characterized. The effect of changing the concentration and the excitation power on the nonlinear properties was studied using the Z-scan technique. The samples have been observed to show self-defocusing, saturable absorption, and reverse saturable absorption. The negative sign of nonlinear refractive index n_2 suggests that nonlinearity is of a thermal lensing origin. The nonlinear absorption coefficient has been observed to change signs from negative to positive with increasing power. Yellow dyes of Tartrazine-Carmoisine solutions are promising for applications in all-optical switching devices.

ACKNOWLEDGMENT

Throughout the making of this project, I have been fortunate to come by plenty of aid and assistance. Thus, I would like to express my gratitude and recognition.

First and foremost, I would like to offer my special thanks to my supervisor Dr. Khalil Ebrahim Jasim for his mentorship, endless support, and guidance. I have learned many things working with Dr. Jasim in the laboratory, everything from turning knobs for mirror adjustment, to making effective Zscan measurements. The quality of this work has been greatly elevated in attribute to his expertise.

I would especially like to thank Basmah Salman for her constant engorgement as well as her insightful comments and the many helpful discussions over the years.

Finally, my appreciation extends to my family and friends for their motivation.

REFERENCES

- M. Zidan, Z. Ajji, A. Allaf, and A. Allahham, "Optical limiting behavior of c60 doped ethylenepropylenediene polymethylene polymer," *Optics* & *Laser Technology*, vol. 42, no. 4, pp. 600–603, 2010.
- [2] G. Stegeman, E. M. Wright, N. Finlayson, R. Zanoni, and C. Seaton, "Third order nonlinear integrated optics," *Journal of lightwave technology*, vol. 6, no. 6, pp. 953–970, 1988.
- [3] K. E. Jasim, "Third-order nonlinear optical properties of quantum dots," in Standards, Methods and Solutions of Metrology. IntechOpen, 2019.
- [4] A. Azarpour, S. SHarifi, and M. Khzaei-Nezhad, "Study of nonlinear optical properties of saffron in nano-droplet and solvent by the single beam z-scan technique," *Optoelectronics, Instrumentation and Data Processing*, vol. 54, no. 1, pp. 32–38, 2018.

- [5] F. Henari, S. Cassidy, K. E. Jasim, and A. Dakhel, "Nonlinear refractive index measurements of curcumin with cw laser," Journal of Nonlinear Optical Physics & Materials, vol. 22, no. 02, p. 1350017, 2013.
- [6] F. Henari and A. Al-Saie, "Nonlinear refractive index measurements and self-action effects in roselle-hibiscus sabdariffa solutions," Laser physics, vol. 16, no. 12, pp. 1664-1667, 2006.
- [7] M. Sheik-Bahae, A. A. Said, T.-H. Wei, D. J. Hagan, and E. W. Van Stryland, "Sensitive measurement of optical nonlinearities using a single beam," IEEE journal of quantum electronics, vol. 26, no. 4, pp. 760-769, 1990.
- [8] F. L. Pedrotti, L. M. Pedrotti, and L. S. Pedrotti, Introduction to optics. Cambridge University Press, 2017.
- [9] T. H. Maiman et al., "Stimulated optical radiation in ruby," 1960.
- [10] J. Hawkes and I. Latimer, Lasers: theory and practice. Prentice Hall,
- [11] R. W. Boyd, Nonlinear optics. Academic press, 2020.
 [12] e. P. Franken, "Ae hill, cw peters, and g," Weinreich. Generation of optical harmonics. Phys. Rev. Lett, vol. 7, pp. 118-119, 1961.
- [13] D. J. Griffiths, "Introduction to electrodynamics," 2005.
- [14] L. I. of America, "American national standard for safe use of lasers ansi z136. 1-2014," 2014.
- [15] F. L. S. Cuppo, A. M. F. Neto, S. L. Gómez, and P. Palffy-Muhoray, "Thermal-lens model compared with the sheik-bahae formalism in interpreting z-scan experiments on lyotropic liquid crystals," JOSA B, vol. 19, no. 6, pp. 1342-1348, 2002.
- [16] C. Gayathri and A. Ramalingam, "Studies of third-order optical nonlinearities and optical limiting properties of azo dyes," Spectrochimica Acta Part A: Molecular and Biomolecular Spectroscopy, vol. 69, no. 3, pp. 980-984, 2008.